Reprinted from THE PHYSICAL REVIEW, Vol. 97, No. 6, 1544–1556, March 15, 1955
Printed in U. S. A.

Equation of State of Metals from Shock Wave Measurements*

JOHN M. WALSH AND RUSSELL H. CHRISTIAN†
Los Alamos Scientific Laboratory, Los Alamos, New Mexico

(Received October 21, 1954)

Shock wave pressure magnitudes from about 150 to 500 kilobars have been attained for metals by using high explosives. A photographic technique for the nearly simultaneous determination of shock and free surface velocities is presented, and measurements for aluminum, copper, and zinc are given.

Expressions are derived which permit the calculation of pressure-compression points from measured velocity pairs. Consequent Hugoniot curves are presented, probable errors for which are 1 to 2 percent in compression for a given pressure. Finally, the known Hugoniot curves are employed in a calculation which determines temperatures and isotherms.

I. INTRODUCTION

WHEN a detonation wave interacts with an explosive-metal interface, a compression wave is transmitted into the metal. In the ordinary case this disturbance is a shock wave separating a compressed state from the undisturbed metal. The pressures attained behind such shock waves are typically in the range 150 to 500 kilobars (1 kilobar $=10^9$ dynes/cm^2 $=986.9$ atmospheres). The associated problem of determining pressure-compression data from shock wave measurements is the subject of the present investigation. Such data serve to supplement and extend the wealth of static pressure-compression data which exist for pressures up to 100 kilobars.[1]

Two basic assumptions are employed throughout the present considerations. First, since shock pressures are several hundred times yield points of the materials involved, an ordinary "fluid" type equation of state is assumed, i.e., a functional relationship (unspecified) between P, V, and T is assumed to be an adequate representation of the metal. This assumption precludes the explicit treatment of effects arising from the material rigidity which, however, are felt to play a

* Work done under the auspices of the U. S. Atomic Energy Commission. Papers on this subject were presented by the authors at the July, 1953 meeting of the Fluid Dynamics Section of the American Physical Society at State College, Pennsylvania and at the 1954 annual meeting of the American Physical Society.

† Now at the University of California Radiation Laboratory, Livermore, California.

[1] See P. W. Bridgman, Revs. Modern Phys. 18, 1–93 (1946) for a general review.

negligible role in the description of states in the present pressure range.

Second, thermodynamic equilibrium is assumed for the calculation of states behind the shock front. Specifically, it is assumed that in a time of 10^{-7} second or less thermodynamic equilibrium is essentially complete.[2] 10^{-7} second corresponds to a shock propagation distance of a few tenths of a millimeter, so that the condition is equivalent to assuming the shock front thickness is a few tenths of a millimeter or less. Application of the Rankine-Hugoniot equations is exact, of course, regardless of the thickness of the shock front. The limitation is imposed because of the finite scale of experimentation: shocks were measured after propagation distances as small as ten millimeters and free surface velocities were measured in the first two or three millimeters of travel. For such geometries the 10^{-7}-second figure is sufficiently small to assure that transient phenomena do not affect the measurements so that measured velocities transform to describe an *equilibrium* state behind the shock wave. An equilibrium time greater than about 10^{-6} second, on the other hand, could cause transient phenomena which would not be detected experimentally, i.e., measured velocities would transform to describe a *quasi-equilibrium* state behind the lead part of the shock front. It seems probable that polymorphic transitions, such as Professor Bridgman has observed for various substances, could in some instances require times in excess of 10^{-6} second. No such transitions have been observed in static experimentation for the substances reported herein and it is assumed that none occur. In the above sense, however, present shock-determined equation-of-state data are *dynamic* data which would differ from corresponding *static* equation of state where equilibrium times in excess of about 10^{-6} second are involved.

Experimental data consist of the accurate measurement of two velocities associated with the shock wave; these are the velocity of the wave as it approaches the free surface of the metal plate (shock velocity) and the initial velocity of the plate free surface when the shock is reflected at this surface as a rarefaction wave (free-surface velocity). Figure 1 illustrates these velocities and certain symbols to be used below. A method for such measurements and data for a series of experiments on aluminum, copper, and zinc are given as Sec. II.

Transformation of the measured velocity pairs to pressure-compression points is immediate (a straightforward application of the first two Rankine-Hugoniot equations) if one approximates the particle velocity behind the shock as one-half the measured free surface velocity. Section III is therefore devoted to establishing the validity of this approximation, where expressions for maximum possible errors associated with its use are derived. Such errors, as applied to present data, are always less than one percent in compression at a given pressure.

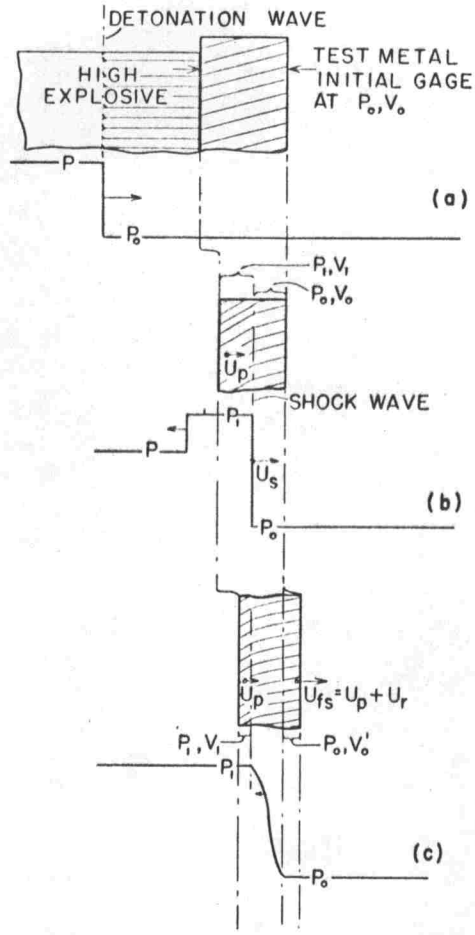

FIG. 1. Schematic illustration of pressure profiles at successive times. Symbols employed are P, $V(\equiv 1/\rho)$ for pressure and specific volume; U_s, U_p, U_r, U_{fs}, for shock velocity, shock-particle velocity, particle velocity due to the rarefaction wave, and free-surface velocity.

The relatively small effect of temperature upon metal compressibility allows the precise determination of related pressure-compression curves, (e.g., adiabats and isotherms neighboring the Hugoniot) by the application of small temperature perturbations. This procedure is given in Sec. IV, where the second TdS equation of thermodynamics and assumptions of constant specific heat (C_v) and $(\partial P/\partial T)_V$ are used to formulate a basis for calculation.

II. EXPERIMENTATION

A typical arrangement used for the determination of velocities is illustrated as Figs. 2(a)–(c). The high-

[2] This interval, the transit time for a particle from an initial state of essentially complete thermodynamic equilibrium ahead of the shock to a final state of "essentially complete" thermodynamic equilibrium behind the shock, is necessarily an approximate concept. Its ultimate refinement is contingent on the structure of the shock front (in particular, the manner of approach to thermodynamic equilibrium) from which definitions of "essentially complete" could be made. Even so the concept is a useful one which permits classification as to the order of magnitude of the times involved.

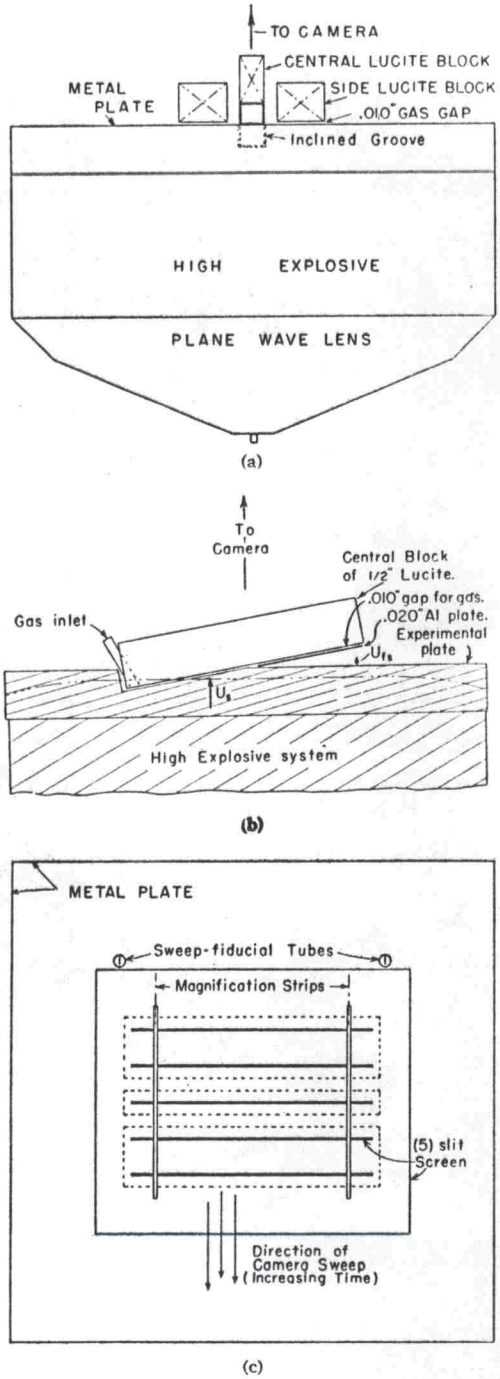

FIG. 2. (a) High explosive system, metal plate, and end view of the Lucite assembly on the free surface of the metal plate. (b) Cutaway side view showing the position of the central Lucite block. (c) Camera view of the assembled shot. The sweep fiducials, end views of which are shown here, are aluminum tubes, approximately $\frac{1}{4}$ in. o.d., $\frac{1}{8}$ in. i.d. by 5 in. long. The far ends of the latter are imbedded about $\frac{1}{4}$ in. in the metal plate; the near ends are pinched to define a small (0.02 in.) aperature.

The slit system consists of a 0.030 in. thick dural plate, into which are machined the 0.040 in. wide slits. The slit system is mounted 1.5 in. in front of, and parallel to, the main plate. The central slit is aligned to view the central Lucite block; the two slits to either side of the central slit are over the side Lucite blocks.

explosive assembly consists of a plane wave lens,[3] followed by a block of high explosive. This assembly induces a strong shock into the machined metal plate, one surface of which is in contact with the high explosive.

Shock and free-surface velocities are recorded by a high-speed sweep camera.[4] Shock velocity is measured as near as possible to the free surface of the plate to minimize effects of shock deceleration, and free-surface velocity is determined for the first few millimeters of run. These measurements are accomplished with an assembly on the free surface of the metal plate, of which the following is typical: A flat bottom groove, 0.5 in. wide, is milled near the center of the free surface at an angle of 10° to the surface. A Lucite block $\frac{1}{2}$ in. $\times 1$ in. $\times 5$ in. is accurately placed in the groove parallel to, but 0.010 in. away from the bottom surface. The lower surface of the Lucite is machined and polished flat, and that portion of the lower surface which protrudes from the groove (about half) is covered by a 0.020 in. dural plate which is spaced 0.010 in. away from the Lucite surface. The pieces are glued together with small shims maintaining the 0.010 in. gaps. This state of assembly is illustrated as Fig. 2(b). Two additional Lucite blocks (1 in. $\times 1$ in. $\times 5$ in.) are similarly fitted alongside the groove, parallel to the free surface of the metal plate but 0.010 in. away from it [see Fig. 2(a)].

As the shock wave reaches the 0.010-in. gaps at the groove bottom and the plate free surface, it causes the metal to move to the Lucite. This process, in turn, causes multiple shock reflections of the gas within the gaps and luminosity results. Air shocks have proved sufficiently luminous in certain experiments, while others (where the metal free surface velocity is low) require the introduction of argon gas in the 0.010-in. gaps. The Lucite surface, under attack by the gas shocks and moving metal surface, quickly becomes opaque, providing a sharp shutter action for the light.

A high-speed moving-image camera views this light through a slit system [Fig. 2(c)], sweeping the image in a direction perpendicular to the slits. The extinction of light due to the opacity of the Lucite is useful here since it prevents the record from one slit being swept over that for lower slits.

Traces from all but the central slit merely record times of arrival of the shock wave at various positions on the free surface of the metal; such information must be incorporated in the record to correct for yaw and curvature of the "plane" wave. For the central trace, that half corresponding to the groove in the plate gives

[3] These plane wave generators are a lens-type combination of two explosives with slow and fast detonation velocities, such that point initiation is converted into a plane detonation wave. See J. H. Cook, Research (London) 1, 474 (1948).

[4] The sweep camera used in present investigations is an $f=11$ synchronous rotating-mirror camera capable of writing speeds as high as 3.2 millimeters on the film per microsecond. Photographic records are taken on glass plates (4 in. $\times 5$ in.) to minimize uncertainties associated with film shrinkage.

a record of shock velocity as the shock wave approaches the free surface. The other half of this trace is caused by the collision of the plate with the Lucite assembly protruding from the groove; i.e., by closing the 0.010-in. gap defined by the bottom surface of the Lucite and the 0.020-in. aluminum. This half of the trace constitutes a record of free-surface motion. The primary purpose of the 0.020-in. aluminum cover plate is to prevent light from the relatively weak air shocks ahead of the metal free surface from writing on the record. It is possible, however, to eliminate the 0.020-in. plate and measure the trailing edge of the resultant film trace. Velocities so obtained agree within experimental error with those measured by the present method.

The direction of increasing time is conveniently and accurately fixed on the record by two long tubes [see Fig. 2(c)] embedded (about $\frac{1}{4}$ in.) in the metal plate above the Lucite. Brilliant jets within the tubes, viewed by the camera through small holes in the tube ends, register sweep direction on the sides of the film. Finally, the images on the record of small metal strips placed across the slits (at known spacing) serve to fix the scale (or magnification number) for the record.

The assembly is mounted for firing on a wooden base, and plywood shields (defining a small window through which the camera views the slit plate and the sweep fiducials) are incorporated to protect the record from stray light for the ten or so microseconds until the changing field of view of the sweep camera no longer coincides with the exploding assembly. The camera and its operators are in an underground chamber some 15 feet away.

TABLE I. Experimental data.

Material	Explosive block (in.)	Plate thickness (in.)	Shock velocity, U_s (mm/μsec)	Free-surface velocity, U_{fs} (mm/μsec)
24 ST aluminum				
$\rho_0=2.785$ g/cm³	2 (thick) Baratol	1	6.28	1.530
$\alpha=72\times10^{-6}$/°C	2 (thick) Baratol	1	6.32	1.522
$C_p=0.22$ cal/g°C	4 (thick) Baratol	1	6.34	1.550
$C_v=0.22$ cal/g°C	2 Composition B	2	6.86	2.280
$(\partial P/\partial T)_V=50.6\times10^6$	2 Composition B	1	7.12	2.607
dynes/cm²°C	2 Composition B	1	7.12	2.551
	2 Composition B	1	7.14	2.563
	4 Composition B	1	7.27	2.792
	4 Composition B	1	7.26	2.854
	4 Composition B	½	7.41	3.091
	6 Composition B	½	7.47	3.140
	6 Composition B	½	7.46	3.112
	8 Composition B	½	7.52	3.250
	12 Composition B	½	7.53	3.292
2 S aluminum	4 (thick) Baratol	1	6.42	1.627
$\rho_0=2.706$	2 Composition B	2	6.94	2.355
$\alpha=72\times10^{-6}$/°C	4 Composition B	1	7.44	2.931
$C_p=0.22$ cal/g°C	8 Composition B	½	7.58	3.250
$C_v=0.22$ cal/g°C				
$(\partial P/\partial T)_V=50.6\times10^6$ dynes/cm²°C				
Zinc				
$\rho_0=7.14$ g/cm³	4 (thick) Baratol	1	4.019	1.345
$\alpha=110\times10^{-6}$/°C	2 (thick) Baratol	1	3.850	1.230
$C_p=0.095$ cal/g°C	2 Composition B	1	4.418	1.684
$C_v=0.095$ cal/g°C	4 Composition B	1	4.663	2.016
$(\partial P/\partial T)_V=70\times10^6$	6 Composition B	1	4.684	2.085
	6 Composition B	½	4.791	2.241
	12 Composition B	½	4.792	2.344
	8 Composition B	½	4.815	2.394
Copper	2 (thick) Baratol	2	4.556	0.920
$\rho_0=8.903$ g/cm³	4 (thick) Baratol	1	4.525	0.919
$\alpha=53\times10^{-6}$/°C	4 TNT	½ Brass, ½ Dural	4.768	1.094
$C_p=0.093$ cal/g°C				
$C_v=0.093$ cal/g°C	4 TNT	½ Brass, ½ Cu	4.769	1.099
$(\partial P/\partial T)_V=75.5\times10^6$ dynes/cm²°C	2 Composition B	2	4.94	1.343
	2 Composition B	1	4.913	1.367
	4 Composition B	1	5.258	1.645
	3 Composition B	1	5.128	1.560
	3 Composition B	½	5.240	1.670
	6 Composition B	1	5.285	1.710
	12 Composition B	½	5.391	1.927
	12 Composition B	½	5.397	1.937

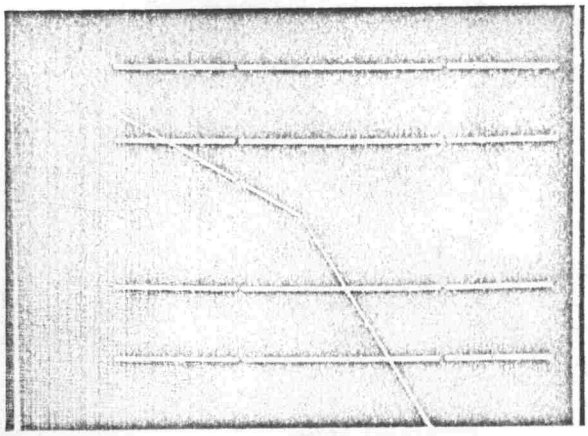

FIG. 3. A photographic record. Vertical side streaks record the direction of increasing time. The four horizontal traces record relative times of arrival of the shock wave at the plate free surface. Slanting lines are velocity traces for the shock and free surface motions. Breaks in the reference lines correspond to positions of magnification tapes.

A photographic record is given as Fig. 3, where pertinent features are identified.

The analysis of the record is accomplished with a Gaertner comparator which measures to one micron in both horizontal and vertical directions. First, the film is accurately aligned so that the vertical direction of cross-hair travel corresponds to the sweep direction (determined by the side streaks). Readings are made by recording the vertical scale positions of all lines (including the shock or free surface line) for each of a series of horizontal scale readings. Reference slit readings for each vertical line are then interpolated to determine the corresponding value for the central slit. The differences between each of these values and the corresponding value of the shock velocity line (or free surface velocity line) then constitute data for distance (along the central slit) *versus* time plots, vertical differences being readily converted to times by knowledge of camera writing speed. Each point on these plots is defined by measurements which affect only that point, so that the method of least squares is appropriately used to determine the best (straight line) fits. Velocities corresponding to the slopes are then the phase velocities of interception of the shock wave with the 10° groove and the free surface with the 10° wedge, which can be readily converted to true shock and free surface velocities.

Experimental data are listed in Table I and presented graphically as Fig. 4. Probable errors for individual velocity determinations are of the order of 0.5 percent.

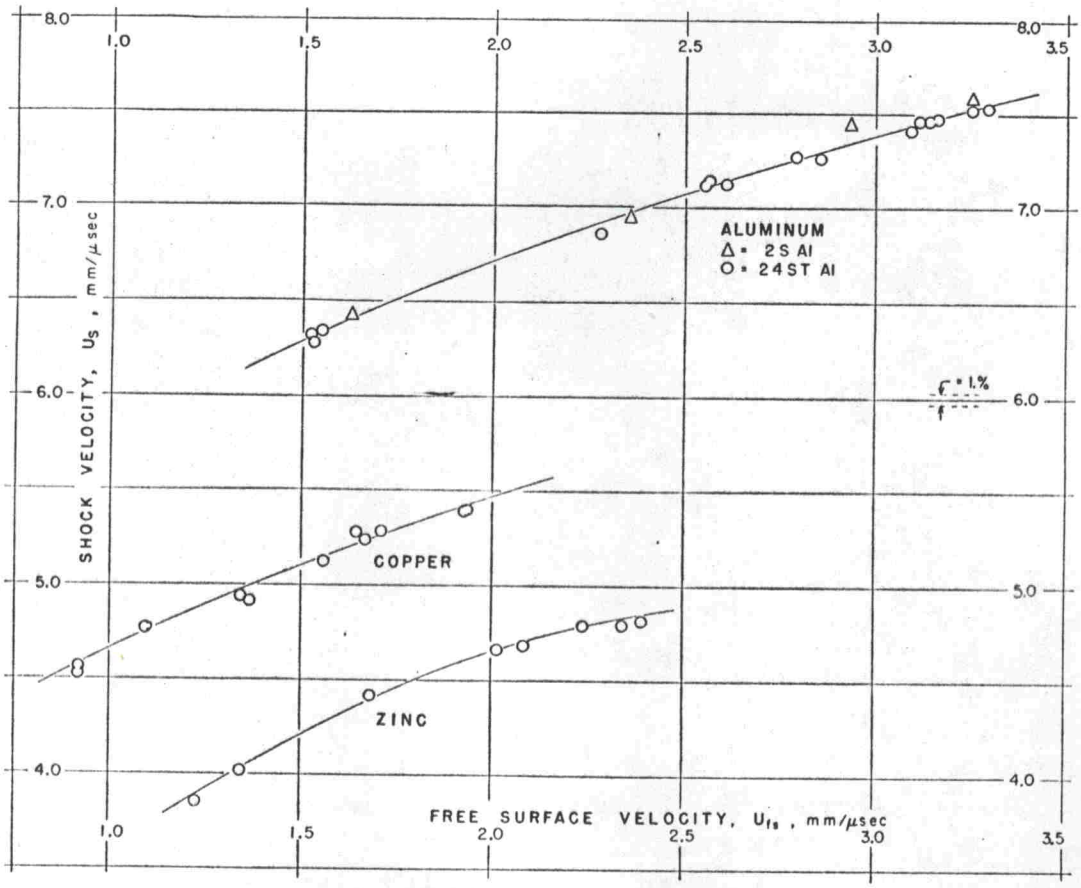

FIG. 4. Experimental data. See also Table I.

Most of this error (about 0.4 percent) is ascribed to shot assembly uncertainties. Tolerances in this phase of the work are accordingly low, all measurements in the Lucite-metal assembly being made to 0.0001 in. Uncertainty in the analysis is 0.1 percent to 0.5 percent, depending upon record quality. Assembly and analysis measurements are made individually for each experiment, so that the resultant errors should be random and represented by scatter in the final data. Camera writing speed, however, is applied in the determination of all velocities. This parameter has been measured to better than 0.2 percent and is therefore believed to be eliminated as the only possible source of significant consistent error in the determination of velocities.

III. DETERMINATION OF HUGONIOT CURVES FROM EXPERIMENTAL DATA

A. Basic Equations[5]

The conservation equations for a shock wave are

$$\rho_0 U_s = \rho_1 (U_s - U_p), \quad \text{Mass} \quad (1)$$

$$P_0 + \rho_0 U_s^2 = P_1 + \rho_1 (U_s - U_p)^2, \quad \text{Momentum} \quad (2)$$

$$E_1 - E_0 = \tfrac{1}{2}(P_1 + P_0)(V_0 - V_1), \quad \text{Energy} \quad (3)$$

which, together with their immediate consequences,

$$V_1/V_0 = (U_s - U_p)/U_s, \quad (4)$$

$$P_1 = \rho_0 U_s U_p + P_0, \quad (5)$$

$$U_p = [(P_1 - P_0)(V_0 - V_1)]^{\frac{1}{2}}, \quad (6)$$

will be used below.

Similarly, from the governing equations for continuous adiabatic flow (mass and momentum conservations), the expression

$$U_r = \int_0^{P_1} \left[\left(-\frac{dV}{dP} \right)^{\frac{1}{2}} dP \right]_{\text{adi}} \quad (7)$$

for the particle velocity due to a centered simple rarefaction wave can be derived. The subscript "adi" is used to denote integration along a line of constant entropy.

In the present problem the material velocity behind the rarefaction wave (this velocity corresponds to the measurable free surface velocity, U_{fs}, referred to the laboratory system of coordinates) is the sum of that due to the shock and that due to the rarefaction wave,

[5] Equations (1)–(7) are derived in any treatise on shock-wave hydrodynamics. See, for example, R. Courant and K. O. Friederichs, *Supersonic Flow and Shock Waves* (Interscience Publications, New York, 1948), where Eq. (7), in particular, can be obtained from their Eq. (34.05).

i.e.,

$$U_{fs}=U_p+U_r. \tag{8}$$

The approximate relation,

$$U_r/U_p \doteq 1, \tag{9}$$

combined with Eqs. (8), (4), and (5) suffices to determine a P_1, V_1 point per set (ρ_0, U_s, U_{fs}) of experimental data. The investigation of this approximation constitutes the next two subsections, where expressions for extreme possible ratios are developed.

B. Maximum Possible Value of U_r/U_p

Consider a substance which is shocked from the initial state (P_0,V_0) to some point (P_1,V_1) on the Hugoniot curve (see Fig. 5) and then relieved adiabatically to a point $(P_0'V_0')$. The gain in specific internal energy due to the shock is given by Eq. (3), while the loss upon adiabatic expansion is $\int[-PdV]_{adi}$ evaluated along the adiabat. The difference between final and initial internal energy is therefore

$$E'-E_0=\frac{P_1+P_0}{2}(V_0-V_1)-\int_{V_1}^{V_0'}[Pdv]_{adi}. \tag{10}$$

Initial and final pressures in the present applications (P_0 is the pressure of the atmosphere, P_0' is the pressure of the air shock ahead of the moving metal free surface) are essentially zero. For this condition values of the specific heat (c_p) and the thermal coefficient of volume expansion (α) are available from handbook tabulations. Thus

$$E_0'-E_0=C_p(T_0'-T_0)=(C_p/\alpha V_0)(V_0'-V_0). \tag{11}$$

Equating (10) and (11) and substituting the identities

$$V_0'=V_1-\int_0^{P_1}\left[\frac{dV}{dP}dP\right]_{adi},$$

$$\int_{V_1}^{V_0'}[PdV]_{adi}=\int_0^{P_1}[VdP]_{adi}-P_1V_1,$$

then yields

$$\int_0^{P_1}\left[\left(V-\beta\frac{dV}{dP}\right)dP\right]_{adi}=\frac{P_1(V_0+V_1)}{2}+\beta(V_0-V_1), \tag{12}$$

$$\beta=\frac{C_p}{\alpha V_0},$$

for an expression of the fact that the total change in specific internal energy is zero around a closed cycle (in this case 010′0, Fig. 5).

We now seek, employing known results from the calculus of variations, that adiabat which produces an extreme value of U_r. Specifically, we seek that curve $V(P)$ between the point P_1, V_1 and the line $P=0$ (but otherwise arbitrary) which produces an extremum of the right side of Eq. (7) and also satisfies the accessory condition defined by Eq. (12).

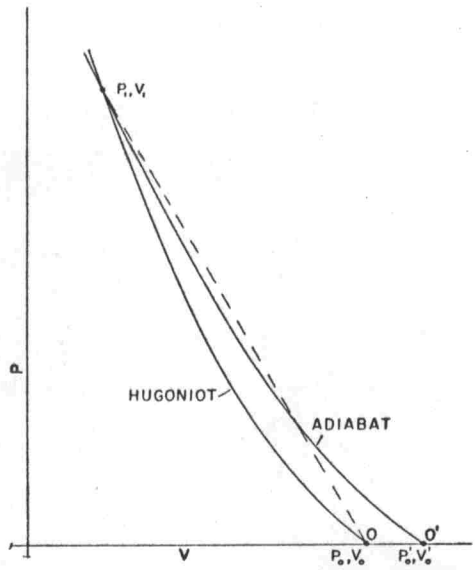

FIG. 5. $P-V$ plot showing relative positions of the Hugoniot and a pressure-release adiabat.

The linear combination of integrands is[6]

$$K=\left(-\frac{dV}{dP}\right)^{\frac{1}{2}}-\lambda\beta\frac{dV}{dP}+\lambda V,$$

where λ is an undetermined multiplier. The associated Euler equation is

$$\frac{d}{dP}\left[\frac{1}{2}\left(-\frac{dV}{dP}\right)^{-\frac{1}{2}}+\lambda\beta\right]=-\lambda.$$

Successive integration yields

$$(V-b)(P-a+\beta)=1/4\lambda^2.$$

This relation is subject to the three conditions

$$V=V_1 \quad \text{at} \quad P=P_1, \qquad \frac{\partial K}{\partial(dV/dP)}=0 \quad \text{at} \quad P=P_0,$$

and Eq. (12), which suffice to determine a, b, and λ. The resulting $P-V$ curve is the hyperbola

$$(P+\beta)(V-V_1)+\frac{P-P_1}{P_1+\beta}\frac{(V_0-V_1)(\beta+\frac{1}{2}P_1)}{\ln[(P_1+\beta)/\beta]}=0, \tag{13}$$

and the associated extremum of U_r, from Eq. (7), is

$$(U_r)_{max}=\left[(V_0-V_1)\left(\frac{P_1}{2}+\beta\right)\ln\frac{P_1+\beta}{\beta}\right]^{\frac{1}{2}}. \tag{14}$$

[6] Notation used is that of H. Marganau and G. M. Murphy, *The Mathematics of Chemistry and Physics* (D. Van Nostrand Company, New York, 1943), Chap. VI.

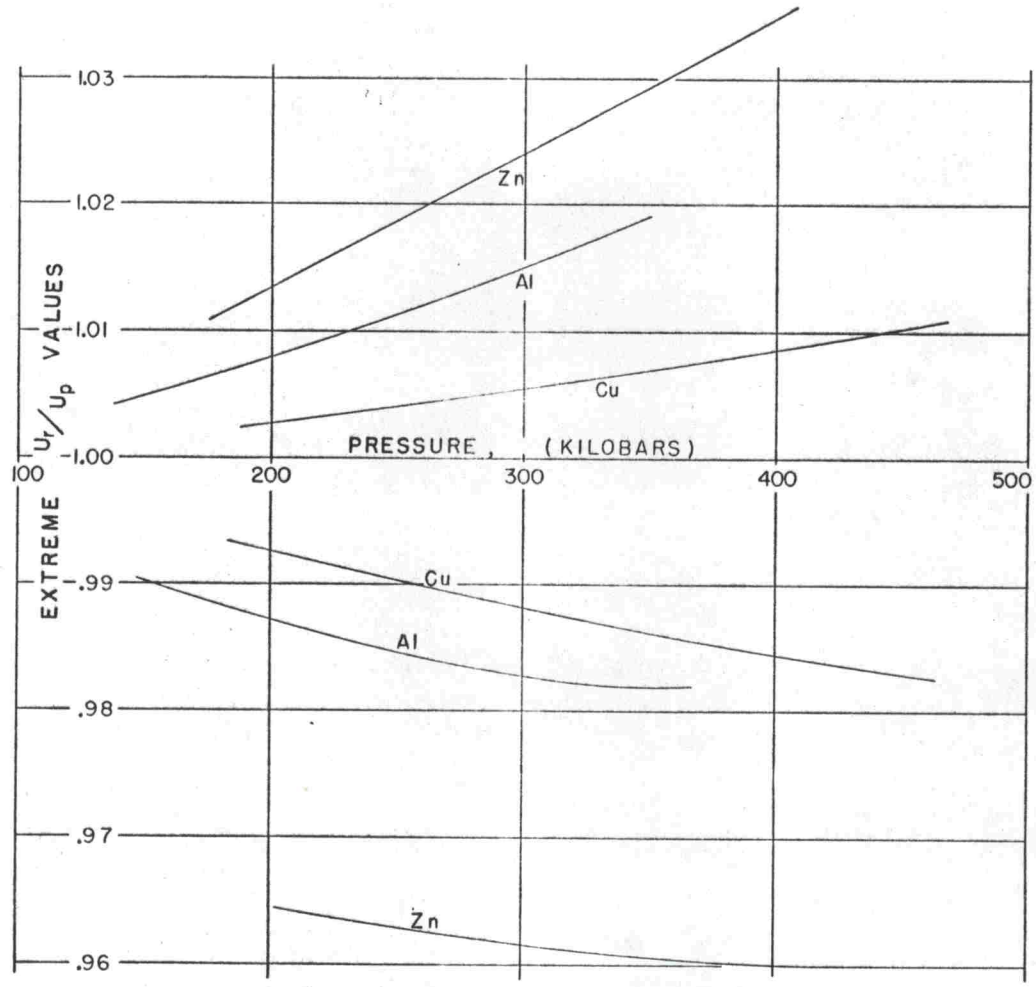

FIG. 6. Maximum and minimum possible U_r/U_p ratios.

This extremum is clearly a maximum since a straight line adiabat from P_1, V_1, to $P=0$, V_0, in particular, satisfies Eq. (12) and yields a smaller U_r. The maximum ratio is

$$\left(\frac{U_r}{U_p}\right)_{\max}=\left[\left(\frac{P_1+2\beta}{2P_1}\right)\ln\left(\frac{P_1+\beta}{\beta}\right)\right]^{\frac{1}{2}}, \quad (15)$$

since U_p does not depend upon the adiabat.

This ratio is unity in the limiting case of zero shock pressure and increases monotonely with P_1. It is also interesting to note that the ratio is independent of V_1; plots of calculated values *versus* P_1 are given in Fig. 6. Values are typically about 1.02 and less than 1.04 in all cases.

The determination for an experiment (set of values ρ_0, U_s, U_{fs}) of the corresponding ratio is not immediate since P_1 is not *a priori* known. The solution is easily attained, however, by a simple process of successive approximations. Unity is assumed for the ratio in order to determine a corresponding pressure through Eqs. (5) and (8). This pressure yields a refined value of the ratio through Eq. (15). This value of the ratio is used to redetermine a pressure, etc. In practice the first-calculated value of the ratio proves sufficiently precise, being accurate to four significant figures in present applications.

C. Minimum Possible Value of U_r/U_p

A minimum for the U_r/U_p ratio can also be established. To this end the following general conditions are imposed upon possible adiabats, $V(P)$, connecting the state P_1, V_1 behind the shock, and the line $P=0$:

$$dV/dP<0, \quad (16)$$

$$d^2V/dP^2>0, \quad (17)$$

$$V(P)\geq V_H(P). \quad (18)$$

The third condition follows from the more basic equation of state condition $\partial V(P,S)/\partial S>0$ and the well-established fact[7] that entropy increases with pressure along the Hugoniot curve $V_H(P)$.

[7] See, for example, Courant and Friedrichs, reference 5, pp. 141–146, where proof is obtained using only conditions equivalent to those enumerated above (i.e., the Bethe-Weyl conditions).

The minimum possible value of U_r compatible with these restrictions corresponds to an adiabat which coincides everywhere with the Hugoniot curve. To prove this, it is sufficient to show that any adiabat $V_I(P)$ which does not everywhere coincide with the Hugoniot curve does not yield the minimum value of U_r, i.e., can be replaced by another curve $V(P)$ for which the associated U_r is smaller: Consider two points P_3, $P_2(P_3>P_2)$ on some segment of the curve $V_I(P)$ which does not coincide with the Hugoniot (i.e., $V_I>V_H$ for $P_3>P>P_2$). Replace the segment of $V_I(P)$ between P_3 and P_2 by

$$V(P)=V_I(P)-\epsilon[(P_3-P)(P-P_2)]^2, \qquad (19)$$

where ϵ is sufficiently small that conditions (16)–(18) are not violated. The contribution to the integral in Eq. (7) for this new segment is

$$\Delta U_r=\int_{P_2}^{P_3}\left(-\frac{dV}{dP}\right)^{\frac{1}{2}}dP=\int_{P_2}^{P_3}\Big[-\frac{dV_I}{dP}$$
$$+2\epsilon(P-P_2)(P_3-P)(P_2+P_3-2P)\Big]^{\frac{1}{2}}dP.$$

The derivative with respect to ϵ may be written:

$$\frac{\partial(\Delta U_r)}{\partial\epsilon}=-\int_{\frac{1}{2}(P_2+P_3)}^{P_3}\frac{(P-P_2)(P_3-P)(2P-P_2-P_3)}{[-dV/dP]^{\frac{1}{2}}}dP$$
$$+\int_{P_2}^{\frac{1}{2}(P_2+P_3)}\frac{(P-P_2)(P_3-P)(P_2P_3-2P)}{[-dV/dP]^{\frac{1}{2}}}dP. \qquad (20)$$

Both integrals in the last equation are positive. Substituting $P=P_2+P_3-Z$ in the second we see that it is identical to the first except that the demominator is greater, by condition (17). Hence

$$\partial(\Delta U_r)/\partial\epsilon<0$$

so that the new segment causes a decrease in ΔU_r and hence a lower value of U_r. Thus no curve $V_I(P)$ which does not everywhere coincide with the Hugoniot yields the minimum value for U_r. It follows that the desired minimum is obtained by integration along the Hugoniot curve

$$(U_r)_{\min}=\int_0^{P_1}\left[\left(-\frac{dV}{dP}\right)^{\frac{1}{2}}dP\right]_{\text{Hug}}, \qquad (21)$$

so that the minimum ratio is

$$(U_r/U_p)_{\min}=\int_0^{P_1}\left[\left(-\frac{dV}{dP}\right)^{\frac{1}{2}}dP\right]_{\text{Hug}}\Big/$$
$$[P_1(V_1-V_0)]^{\frac{1}{2}}. \qquad (22)$$

The subscript "Hug" denotes line integration along the Hugoniot curve.

The determination from experimental data (ρ_0 and the U_s *versus* U_{fs} curve) of the corresponding $(U_r/U_p)_{\min}$ ratios is again most easily accomplished by successive approximations: A "first order" Hugoniot curve is defined by the unity approximation and Eqs. (4), (5), and (8), which curve then permits the calculation of minimum possible ratios (for that curve) from Eq. (22). These ratios are, in turn, employed to redetermine associated curves, etc., a process which can be continued until self-consistency is attained, i.e., until the computed curve regenerates the same ratios which determined its locus in the previous cycle. This process, as applied to present data, is also rapidly convergent, the variation in the calculated ratios being negligible after the first calculation.

Values for the $(U_r/U_p)_{\min}$ are given in Fig. 6 where they are plotted *versus* shock pressure. These values, typically about 0.98, are greater than 0.96 throughout the experimental range.

D. Results

The extrema for U_r/U_p determine associated extreme possible positions for the Hugoniot curve. Comparisons of these extremes and the curve obtained by the free-surface velocity approximation are made graphically as Fig. 7. Neither extreme possible position disagrees with the approximate curve (which lies about half-way between the two) by more than 1 percent in compression ($\Delta V/V_0$) for a given pressure, 0.5 percent being more typical of all data. These uncertainties are sufficiently small to justify the approximation as applied to present

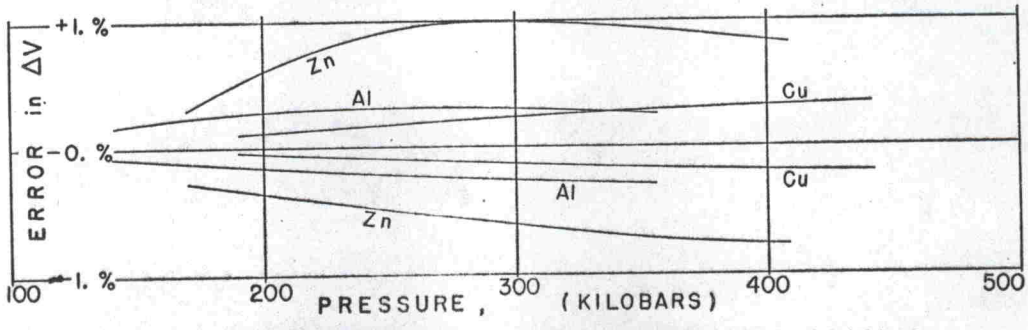

FIG. 7. Maximum possible errors in ΔV associated with the approximation $(U_r/U_p)=1$. Curves above the zero line pertain to the minimum calculation.

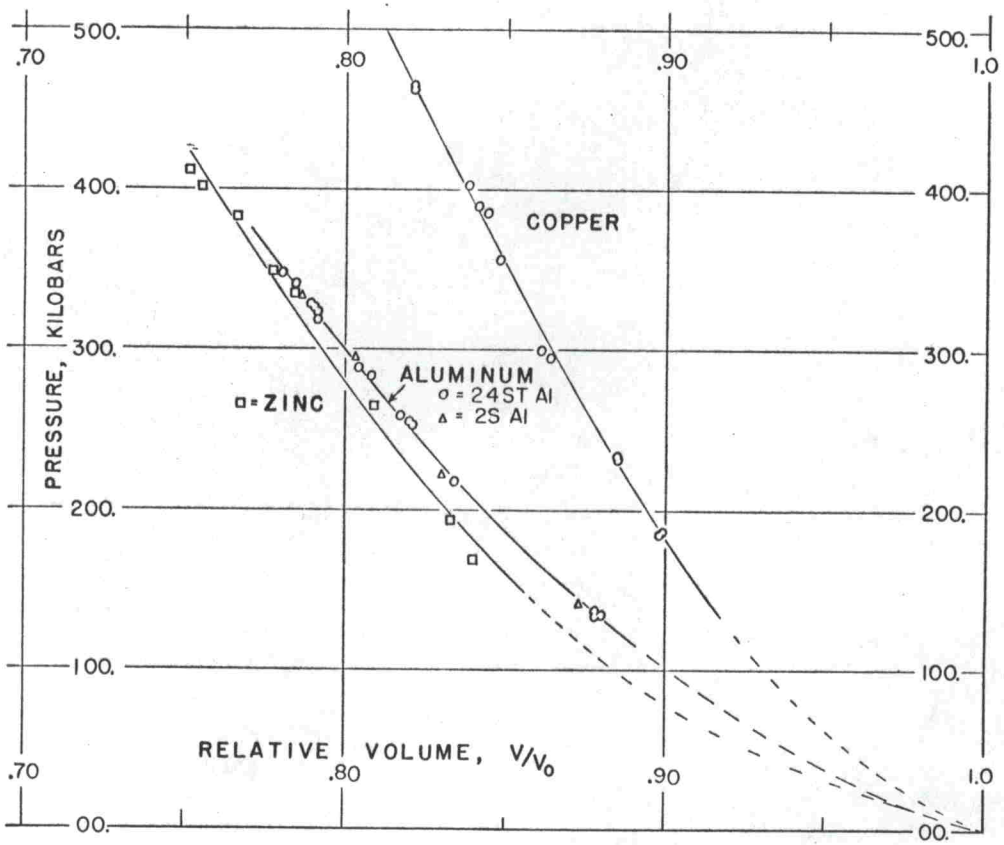

FIG. 8. Hugoniot curves. See also Table II.

data. Resulting data points which determine the Hugoniot curves for aluminum, copper, and zinc are listed as Table II and plotted as Fig. 8.

Over-all precision for experimental Hugoniot points are determined by the accuracy of the above approximation, the precision of the velocity measurements reported in Sec. II, and the transformation equations to the $P-V$ plane. Results may be conveniently summarized as estimated probable errors in compression for a given pressure, as applied to the curves. These over-all uncertainties are estimated at 1 percent for the 24 ST-aluminum curve and 2 percent for the copper and zinc curves.

TABLE II. Pressure relative-volume points.

Material	P (kilobars)	V/V_0	P (kilobars)	V/V_0
24 ST aluminum	133.9	0.878	288.7	0.804
	134.1	0.880	318.9	0.791
	136.8	0.878	326.6	0.790
	218.0	0.834	323.3	0.791
	258.6	0.817	328.4	0.789
	253.2	0.821	340.2	0.784
	254.9	0.820	347.0	0.780
	282.9	0.808		
2 S aluminum	141.3	0.873	295.0	0.803
	221.3	0.830	333.3	0.786
Zinc	193.0	0.833	348.7	0.777
	169.1	0.840	383.5	0.766
	265.6	0.809	401.0	0.755
	335.6	0.784	411.5	0.751
Copper	186.6	0.899	356.1	0.848
	185.1	0.898	385.0	0.844
	232.1	0.8853	389.5	0.841
	233.4	0.8847	402.3	0.838
	295.3	0.864	462.0	0.821
	299.0	0.861	465.4	0.821

IV. TEMPERATURE CALCULATIONS. DETERMINATION OF ISOTHERMS

The thermodynamic identity

$$TdS=C_v dT+\left(\frac{\partial P}{\partial T}\right)_V TdV \tag{23}$$

permits, for known C_v and $(\partial P/\partial T)_V$, the calculation of temperatures along Hugoniot curves and adiabats. For present applications, both C_v and $(\partial P/\partial T)_V$ are assumed constant. These assumptions, suggested by the insensitivity of both parameters to pressure and temperature in static compressibility work, are presumed adequate to permit the approximate calculation of temperatures and the small offsets between $P-V$ curves of different temperatures. For present purposes, it is interesting to calculate the temperatures along the Hugoniot curve, the final temperature after the material

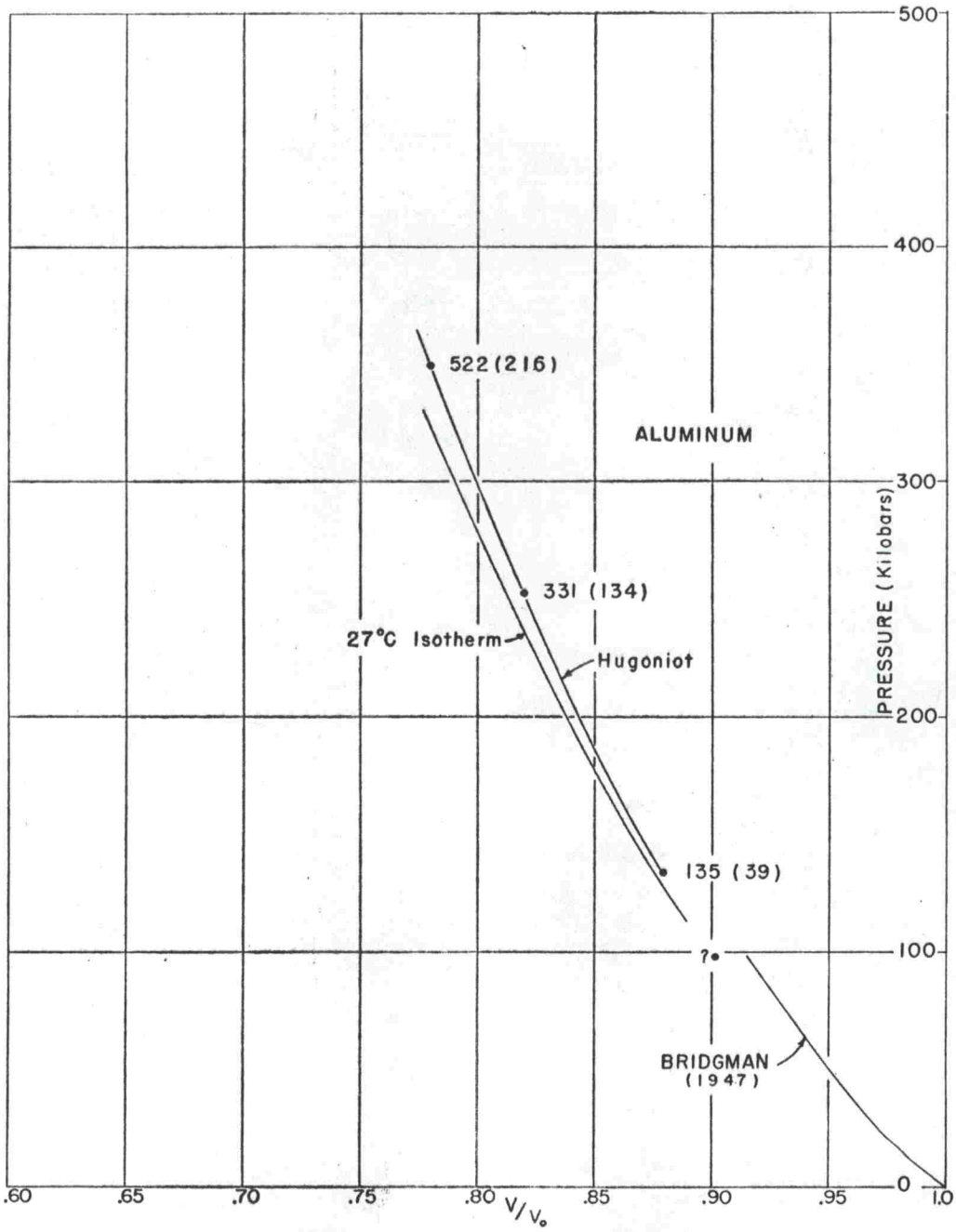

FIG. 9. Temperatures and isothermal compressions for aluminum. Numbers along Hugoniot curve give temperature rise (°C) associated with a shock of corresponding magnitude. Neighboring numbers in parentheses correspond to temperature rise associated with the combined shock and rarefaction processes. An initial temperature of 27°C and the thermodynamic data listed in Table I were assumed. The point marked (?) was also reported by Professor Bridgman who expressed greater credence for the curve drawn.

has been relieved adiabatically to zero pressure, and the $P-V$ locus of one (the 27°C) isotherm. Determination of this isotherm involves sufficiently small temperature perturbations that continuity comparisons between statically determined isotherms and those reported here can be made.

Combining Eq. (3) and the first law of thermodynamics we get

$$\int_{S_0}^{S_1}[TdS]_{\text{Hug}}=\frac{P_1+P_0}{2}(V_0-V_1)+\int_{V_0}^{V_1}[PdV]_{\text{Hug}}.$$

Differentiation of the latter gives

$$\frac{d}{dV_1}\int_{S_0}^{S_1}[TdS]_{\text{Hug}}=\frac{dP_1}{dV_1}\frac{(V_0-V_1)}{2}+\frac{P_1}{2},$$

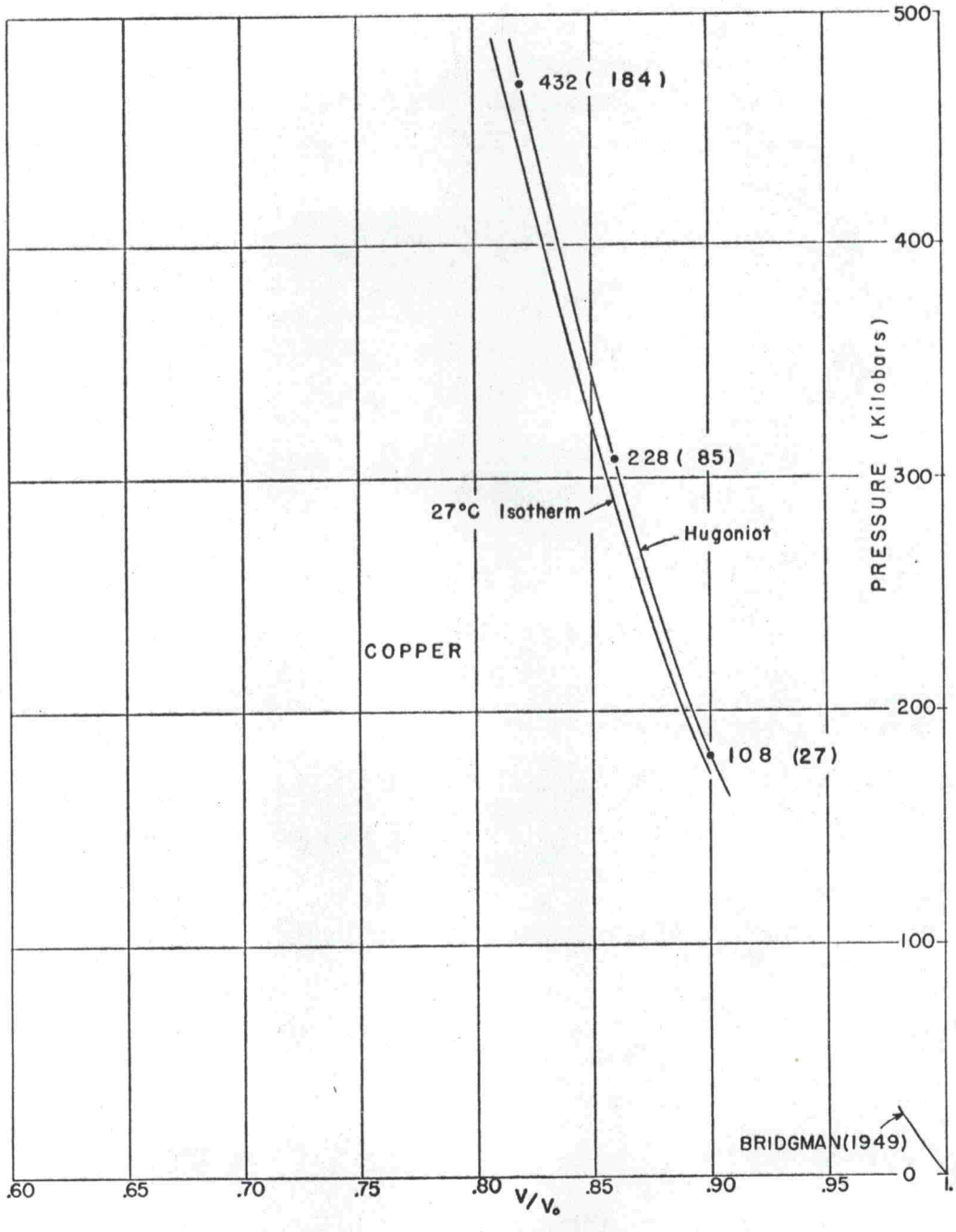

FIG. 10. Temperatures and isothermal compressions for copper.

which, for a given Hugoniot curve, may be written as a function $f(V_1)$. Combining this result with Eq. (23) we get

$$\frac{d}{dV_1}\int_{S_0}^{S_1}[TdS]_{\text{Hug}}=C_v\frac{dT_1}{dV_1}+\left(\frac{\partial P}{\partial T}\right)_V T_1=f(V_1),$$

the solution of which is

$$T_1(V_1)=T_0e^{b(V_0-V_1)}+e^{-bV_1}\int_{V_0}^{V_1}\left[\frac{f(V)e^{bV}}{C_v}dV\right]_{\text{Hug}}, \quad (24)$$

where

$$b=\left(\frac{\partial P}{\partial T}\right)_V\Big/C_v, \quad f(V)=-\frac{1}{2}\frac{dP}{dV}(V_0-V)+\frac{1}{2}P,$$

and the condition $T=T_0$ at $V=V_0$ was imposed.

The similar expression for temperature variation along an adiabat is

$$T_a(V)=T_ie^{b(V_i-V)}, \quad (25)$$

where T_i and V_i are initial conditions at some point on

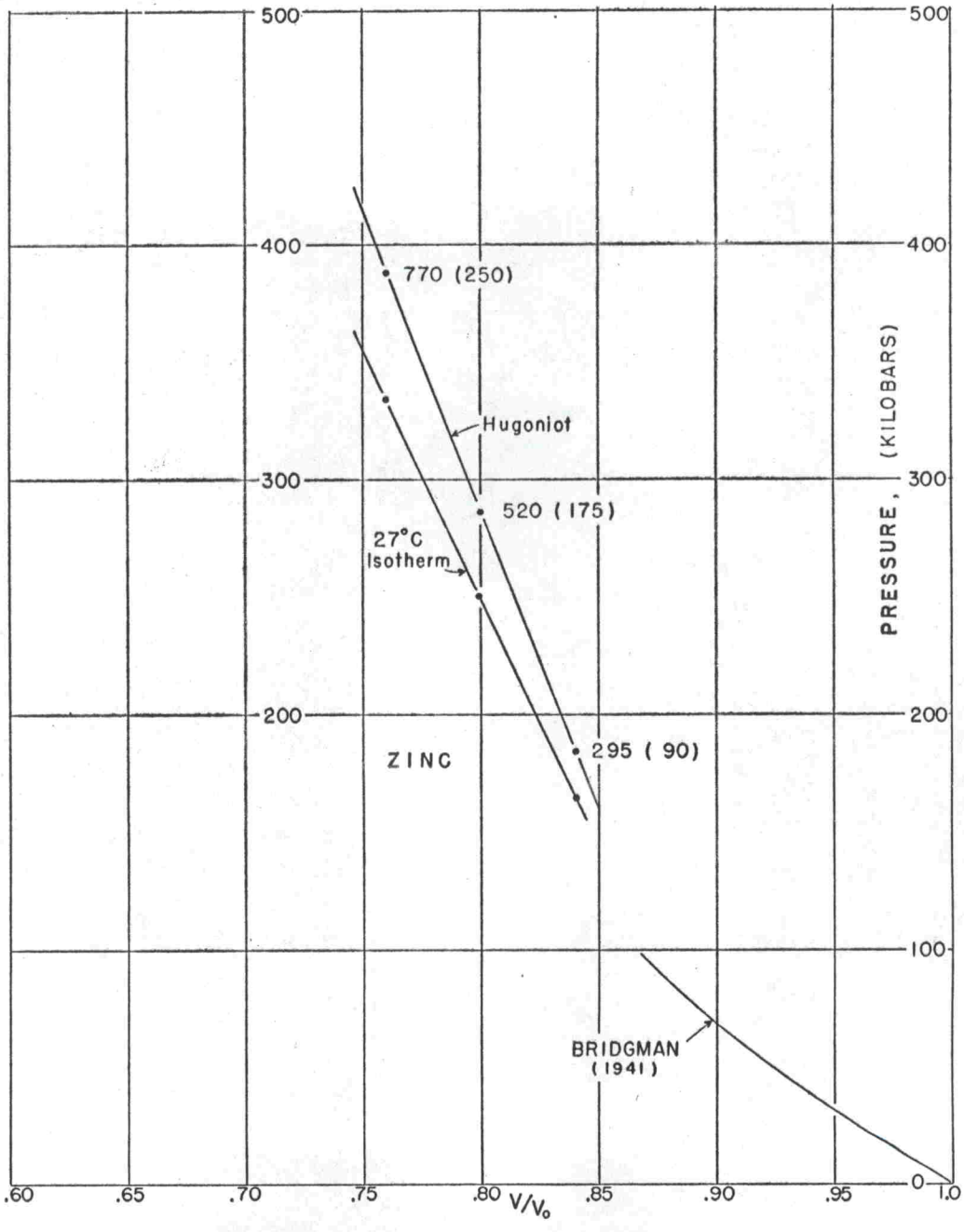

FIG. 11. Temperatures and isothermal compressions for zinc.

the adiabat. This relation follows immediately from Eq. (23). For two points of different T and the same V, the pressure offset is given by

$$\Delta P\Big|_V = \left(\frac{\partial P}{\partial T}\right)_V \cdot \Delta T\Big|_V . \tag{26}$$

Also, for the $P=0$ isobar

$$(V-V_0)_{P=0} = V_0\alpha(T-T_0)_{P=0} \tag{27}$$

relates temperature and specific volume. T_0V_0 refers to normal specific volume and temperature while α is an average value of the thermal coefficient of volume expansion, as before.

Equation (24), augmented by the thermodynamic parameters listed in Table I, was used in straightforward numerical calculations of temperatures along the Hugoniot curves. Results of such calculations are presented in Figs. 9, 10, and 11.

Equation (25) was used in a similar determination of temperatures along pressure-release adiabats. Of particular interest is the final temperature after the material

TABLE III. Calculated adiabats and temperatures. The symbol ΔT means temperature rise, °C, above an assumed initial temperature of 27°C. P is measured in kilobars. The particular adiabat reported for each metal is the one that intersects the Hugoniot curve at the high-pressure end of the latter curve. Temperature rises associated with $P=0$ on the adiabats (where V/V_0 is slightly greater than unity, due to heating) are given as the numbers in parentheses, Figs. 9–11. The determination of additional adiabats (see Sec. IV) involves only a very moderate amount of numerical labor.

	Copper				Aluminum				Zinc			
	Hugoniot		Adiabat		Hugoniot		Adiabat		Hugoniot		Adiabat	
V/V_0	P	ΔT	ΔT	P	V/V_0	P	ΔT	ΔT	P	V/V_0	P	ΔT	ΔT	P
1.0	0	0	194	14.6	1.0	0	0	232	11.7	1.00	0	0	291	20.4
0.98	26	13	216	41.3	0.98	15	12	254	27.2	0.98	9	15	321	30.4
0.96	57	28	239	72.9	0.96	32	27	276	44.6	0.96	20	32	352	42.4
0.94	95	46	263	111.4	0.94	52	44	299	64.9	0.94	34	52	385	57.3
0.92	139	71	288	155.4	0.92	75	65	323	88.0	0.92	51	76	420	75.1
0.90	190	108	314	205.6	0.90	102	95	348	114.8	0.90	73	108	456	97.4
0.88	245	160	342	258.8	0.88	134	135	374	146.6	0.88	100	151	495	124.1
0.86	307	229	370	317.6	0.86	170	184	401	180.9	0.86	133	211	535	155.7
0.84	390	320	400	396.0	0.84	211	247	430	220.5	0.84	175	296	576	194.6
0.82	475	432	432	475.0	0.82	255	331	459	261.5	0.82	225	406	621	240
					0.80	302	419	490	305.6	0.80	280	521	667	290.2
					0.78	350	522	522	350	0.78	335	642	702	339.2
										0.76	390	768	768	390

is relieved adiabatically to zero pressure, obtained by combination of Eq. (25) and Eq. (27). Results of such calculations are also given in Figs. 9–11.

Equation (26) combined with the known $P-V$ locus of the Hugoniot curve and the input temperatures calculated above then permits the immediate determination of isotherms and adiabats neighboring the Hugoniot curve. Resulting 27°C isotherms are plotted in Figs. 9–11 where they may be compared to results of static experimentation.[8–10] A similarly-determined pressure release adiabat (corresponding to a shock strength which is near the strongest attained) is listed for each material as Table III.[11]

[8] P. W. Bridgman, Proc. Am. Acad. Arts Sci. **76**, 55 (1948).
[9] P. W. Bridgman, Proc. Am. Acad. Arts Sci. **77**, 187 (1949).
[10] P. W. Bridgman, Phys. Rev. **60**, 351 (1941).
[11] It is interesting to compute U_r/U_p ratios corresponding to the data given in Table III, an application of Eqs. (6) and (7). These values, 1.017, 1.011, and 1.026 for aluminum, copper, and zinc, are all greater than unity and are fairly close (though slightly less, of course, than the corresponding maxima from Sec. III.) Similar ratios for a material whose Hugoniot exhibits considerable curvature, however (e.g., an organic material), could be less than unity. Corrections to the Hugoniot curve which are indicated by the present ratios (see Sec. IIID) have been neglected.

V. ACKNOWLEDGMENTS

The authors gratefully acknowledge the help of Dr. Clarence M. Fowler and Melvin H. Rice, who participated in the feasibility stage of the present investigation, and of Drs. Robert D. Cowan, William E. Deal, Russell E. Duff, Malcolm E. Ennis, Wildon Fickett, Robert G. Shreffler, and Frank J. Willig, whose encouragement and criticisms were invaluable.

The authors are also indebted to Roy A. Frame, Thomas M. O'Neill, and Frank M. Jackson for their valuable assistance in carrying out the experimentation.